Journal of Biomolecular NMR, **22:** 349–363, 2002.
KLUWER/ESCOM

Automated NMR determination of protein backbone dihedral angles from cross-correlated spin relaxation

Karin Kloiber[a], Wolfgang Schüler[b] & Robert Konrat[c,*]
Institute of Organic Chemistry, University of Innsbruck, Austria

Received 4 February 2002; Accepted 6 February 2002

Key words: chemical shift anisotropy, cross-correlated spin relaxation, dihedral angles, multiple-quantum coherence, NMR spectroscopy, protein structure determination

Abstract

The simultaneous interpretation of a suite of dipole-dipole and dipole-CSA cross-correlation rates involving the backbone nuclei $^{13}C\alpha$, $^{1}H\alpha$,^{13}CO, ^{15}N and $^{1}H^{N}$ can be used to resolve the ambiguities associated with each individual cross-correlation rate. The method is based on the transformation of experimental cross-correlation rates *via* calculated values based on standard peptide plane geometry and solid-state ^{13}CO CSA parameters into a dihedral angle probability surface. Triple resonance NMR experiments with improved sensitivity have been devised for the quantification of relaxation interference between $^{1}H\alpha(i)$-$^{13}C\alpha(i)$/$^{15}N(i)$-$^{1}H^{N}(i)$ and $^{1}H\alpha(i-1)$-$^{13}C\alpha(i-1)$/$^{15}N(i)$-$^{1}H^{N}(i)$ dipole-dipole mechanisms in ^{15}N,^{13}C-labeled proteins. The approach is illustrated with an application to ^{13}C,^{15}N-labeled ubiquitin.

Introduction

NMR cross-correlation spin relaxation rates are now well-established as important sources of structural and dynamic information about molecules in solution. To date, a set of experiments exists, which measures the cross-correlated fluctuations of different dipolar couplings (Reif et al., 1997; Pelupessy et al., 1999; Chiarparin et al., 1999, 2000), dipolar couplings and anisotropic chemical shifts (Yang et al., 1997, 1998; Yang and Kay, 1998; Kloiber and Konrat, 2000a,b, 2001; Sprangers et al., 2000) or different chemical shift tensors (Skrynnikov et al., 2000). Cross-correlated spin relaxation provides unique access to structurally relevant dihedral angles of the protein backbone. The good sensitivity of the spectra allowed applications to systems as large as 42 kDa (Yang et al., 1998). Applications to nucleic acids (Felli et al., 1999; Richter et al., 1999; Boisbouvier et al., 2000; Chiarparin et al., 2001), weakly binding ligands complexed to their receptors (Blommers et al., 1999; Carlomagno et al., 1999) and a catalytic intermediate of a metal-catalyzed substitution reaction (Junker et al., 2000) have also been reported, thus underscoring the general applicability of these methods.

Although there are numerous examples illustrating the sensitivity of the experimental techniques and the accuracy of the obtained dihedral angles (Reif et al., 1997; Yang et al., 1997, 1998; Yang and Kay, 1998; Pelupessy et al., 1999; Chiarparin et al., 1999, 2000; Kloiber and Konrat, 2000a,b; Skrynnikov et al., 2000), a general application, however, is still hampered due to the multiplicity of dihedral angles related to only a single relaxation rate. Approaches to overcome this limitation have been proposed for the dihedral angle ψ (Yang and Kay, 1998) and φ (Kloiber and Konrat, 2000a) by combining measurements from $^{13}C^{\alpha}$-$^{1}H^{\alpha}$ dipolar ^{15}N-$^{1}H^{N}$ dipolar and $^{13}C^{\alpha}$-$^{1}H^{\alpha}$ dipolar $^{13}C'$

*To whom correspondence should be addressed. Institute of Theoretical Chemistry and Molecular Structural Biology, University of Vienna, Rennweg 95b, Austria. E-mail: robert.konrat@univie.ac.at
Present adresses: [a]Protein Engineering Network Centers of Excellence and Department of Medical Genetics and Microbiology, Biochemistry and Chemistry, University of Toronto, Toronto, Ontario, Canada M5S 1A8; [b]ProCeryon Biosciences GmbH, Jakob Haringer Straße 3, A-5020 Salzburg, Austria; [c]Institute of Theoretical Chemistry and Molecular Structural Biology, University of Vienna, Rennweg 95b, Austria.

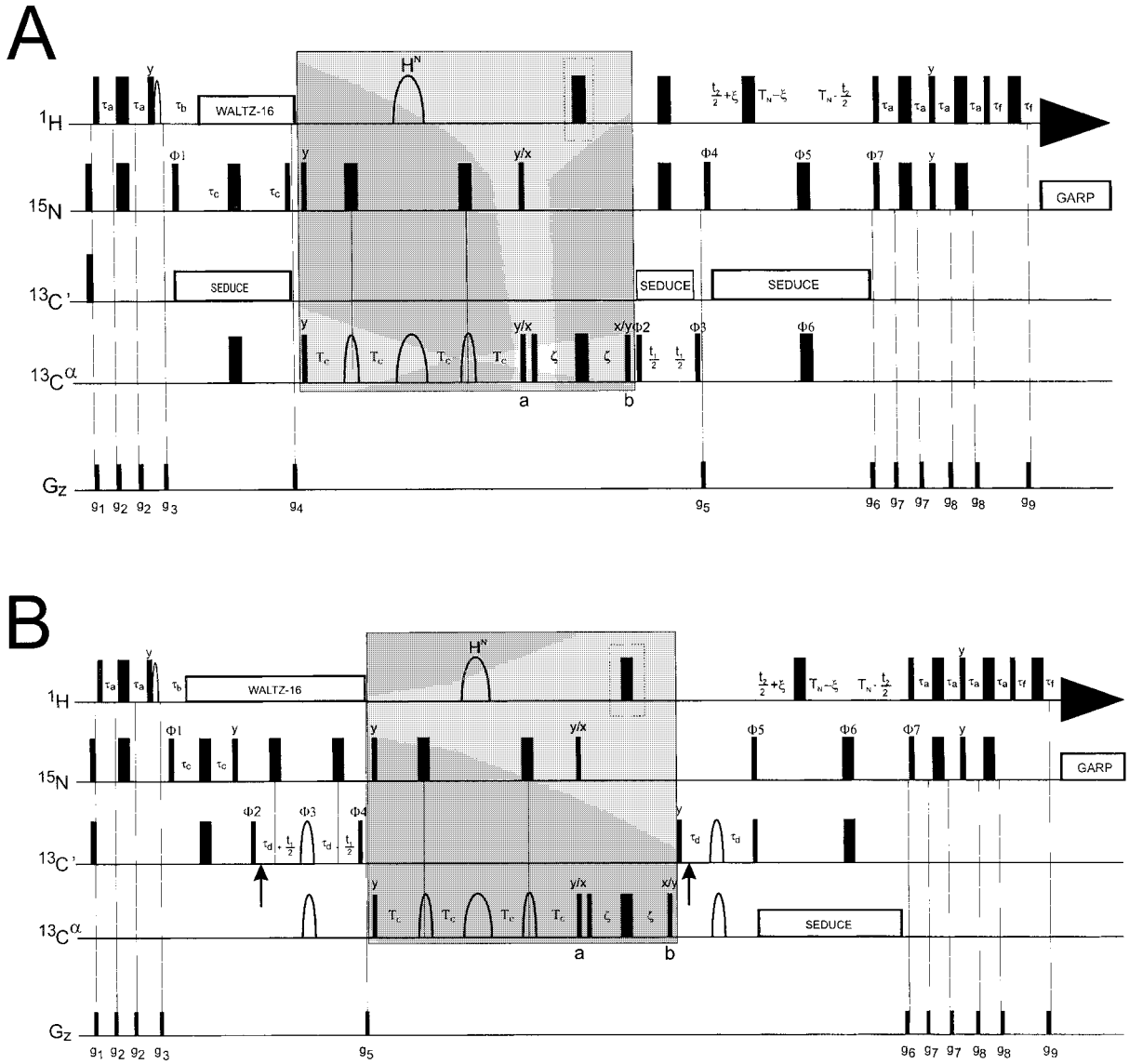

Figure 1. Pulse schemes for the quantification of (A) ^{13}Cα(i)-^{1}Hα(i)/^{15}N(i)-^{1}H^{N}(i) and (B) ^{13}Cα(i−1)-^{1}Hα(i−1)/^{15}N(i)-^{1}H^{N}(i) dipole-dipole relaxation interference in ^{13}C,^{15}N-labeled proteins. Narrow and wide pulses indicate 90° and 180° pulses, respectively, and, unless indicated otherwise, all pulses are applied along the x-axis. The ^{1}H, ^{13}C and ^{15}N carriers were positioned at 4.72 ppm (water), 175 ppm and 119 ppm. The water-selective ^{1}H 90° pulse (after the INEPT period) is applied as a 2.2 ms rectangular pulse, with the carrier on the water resonance. ^{15}N pulses use a 6 kHz field, with GARP (Shaka et al., 1983) decoupling achieved with a 1kHz field. All carbon rectangular pulses employed rf field strengths adjusted $\Delta/\sqrt{15}$, where Δ is the difference between ^{13}Cα and ^{13}C′ chemical shift regions. The ^{13}Cα-^{15}N multiple-quantum evolution period ($4T_C$) is shown in gray. (A) HNCA-type experiment for measurement of ^{13}Cα(i)-^{1}Hα(i)/^{15}N(i)-^{1}H^{N}(i) cross-correlations. ^{13}C′ decoupling during the $^{1,2}J_{NC\alpha}$ evolution delay and the indirect evolution times t_1 and t_2 is achieved with a SEDUCE (McCoy, 1996) decoupling scheme (345 μs, 3 kHz peak rf). ^{13}Cα shaped pulses make use of RE-BURP profiles (Geen and Freeman, 1991). The non-selective ^{13}Cα (also inverting the ^{13}Cβ spins) refocusing pulses (first and third shaped pulses) are 400 μs (15.5 kHz peak rf, excitation centered at 50 ppm), while the selective ^{13}Cα refocusing pulse (second shaped pulse) is of duration 2 ms (3.2 kHz peak rf, excitation centered at 55 ppm). The simultaneous amide inversion pulse was also issued as an RE-BURP (Geen and Freeman, 1991) and centered at 7.9 ppm with 3.09 ms and 2.0 kHz peak rf. Two experiments are recorded which select at time point a in the sequence either $2C_x^{\alpha}N_x$ (reference experiment I) or $8C_y^{\alpha}N_yH_z^{\alpha}H_z^{N}$ (cross experiment II) (see Materials and methods). Experimental conditions for experiment I are as follows: the ^{1}H 180° embraced with brackets is omitted, the phases of the 90° pulses at time points a (^{13}C and ^{15}N) and b (^{13}C) are y and x, and $\xi = 1/(4^{1}J_{NH})$; whereas in experiment II the ^{1}H 180° pulse (in the middle of 2ζ; $\zeta = 1/(4^{1}J_{CH})$ is applied, the phases of the 90° pulses at time points a (^{13}C and ^{15}N) and b (^{13}C) are x and y, and $\xi = 0$. The values for τ_a, τ_b, τ_c, τ_f, ξ and ζ were set to 2.25 ms, 5.3, 12.4, 0.5, 2.63 and 1.78 ms, respectively. $T_C = 6.5$ ms; $T_N = 12.4$ ms. The phase cycling was $\Phi1 = x,-x$; $\Phi2 = x,x,-x,-x$; $\Phi3 = x$; $\Phi4 = y$; $\Phi5 = 4(x),4(-x)$, $\Phi6 = x$;

$\Phi 7 = x$; and the receiver was x,−x,−x,x. Quadrature detection in F_1 is achieved by States-TPPI of Φ3 (Marion et al., 1989) while quadrature in F_2 employs the enhanced sensitivity pulsed field gradient method (Kay et al., 1992; Schleucher et al., 1993) where for each value of t_2 separate data sets are recorded for (g6, Φ7) and (−g6, Φ7 +180°). For each successive t_2 value, Φ4 and the phase of the receiver are incremented by 180°. Gradient levels were as follows: g1=0.5 ms, 8 Gcm^{-1}; g2 = 0.5 ms, 4 Gcm^{-1}; g3 = 1.0 ms, 10 Gcm^{-1}; g4 = 0.5 ms, 8 Gcm^{-1}; g5 = 0.6 ms, 10 Gcm^{-1}; g6 = 1.25 ms, 20 Gcm^{-1}; g7 = 0.5 ms, 8 Gcm^{-1}; g8 = 0.3 ms, 2 Gcm^{-1} and g9 = 0.125 ms, 19.3 Gcm^{-1}. (B) HNCOCA scheme to measure $^{13}C\alpha(i-1)$-$^{1}H\alpha(i-1)/^{15}N(i)$-$^{1}H^{N}(i)$ dipole-dipole relaxation interference. The delay $\tau_d = 1/2J_{C'C\alpha}$ was set to $\tau_d = 11$ ms. Arrows indicate the positions of Bloch-Siegert compensation pulses. $^{13}C\alpha$ decoupling during indirect ^{15}N evolution time t_2 is achieved with a SEDUCE (McCoy and Mueller, 1992) decoupling scheme (345 μs, 3 kHz peak rf). The phase cycling was Φ1 =x,−x; Φ2 = x,x,−x,−x; Φ3 = 8(x),8(y); Φ4 = 4(y),4(−y); Φ5 = y, Φ6 = 4(x),4(−x); Φ7 = x and the receiver was (x,−x,−x,x),(−x,x,x,−x),(−x,x,x,−x),(x,−x,−x,x). Quadrature detection in F_1 is achieved by States-TPPI of Φ2 (Marion et al., 1989) while quadrature in F_2 employs the enhanced sensitivity pulsed field gradient method (Kay et al., 1992; Schleucher et al., 1993) where for each value of t_2 separate data sets are recorded for (g6, Φ7) and (−g6, Φ7 +180°). For each successive t_2 value, Φ5 and the phase of the receiver are incremented by 180°. Gradient levels and other experimental parameters are as in (A).

CSA cross-correlation rates, leading to a reduction in the number of possible ψ,φ values by a factor of 2.

In this report we demonstrate that by a combination of five cross-correlated NMR spin-relaxation rates for the protein backbone nuclei and the $^{3}J_{C'C'}$ scalar coupling constants (related to the dihedral angle φ), an unambiguous determination of the protein backbone dihedral angles is feasible. To this end, we present a new method for the measurement of relaxation interference between $^{1}H\alpha(i)$-$^{13}C\alpha(i)/^{15}N(i)$-$^{1}H^{N}(i)$ and $^{1}H\alpha(i-1)$-$^{13}C\alpha(i-1)/^{15}N(i)$-$^{1}H^{N}(i)$ dipole-dipole mechanisms in ^{15}N,^{13}C-labeled proteins. The new experiments are based on quantitative Γ-spectroscopy and refocus passive $^{1,2}J_{NC\alpha}$ scalar couplings which results in a significant gain in sensitivity. Experimental cross-correlation rates are transformed into a φ(i)/ψ(i−1) dihedral angle probability surface by minimizing a suitable error function. The method is related to a recently proposed graphical construction which also made use of the complementarity of cross-correlation rates measured for two consecutive amino acids and which was demonstrated to resolve contradictions from NMR cross-correlation rates (Tolman et al., 2000).

Materials and methods

All NMR experiments were performed on a Varian UNITY Plus 500 MHz spectrometer equipped with a pulsed field gradient (PFG) unit using a triple resonance probe with actively shielded z gradients. Uniformly ^{13}C,^{15}N-labeled ubiquitin was provided by J. Wand (University of Pennsylvania). The concentration was 1.5 mM, with 50 mM phosphate buffer, pH = 5.5, in 90% H_2O/10% D_2O. All spectra were recorded at 26 °C. The ^{1}H carrier was set to the frequency of the water resonance (4.76 ppm), and the ^{15}N carrier frequency was set to 116 ppm. CSA-dipole cross-correlation rates were measured as described elsewhere (Yang et al., 1997, 1998; Yang and Kay, 1998; Kloiber and Konrat, 2000a). The experiment for the measurement of the relative orientation of successive Cα-Hα bond vectors was performed as published (Chiarparin et al., 2000). The experiment was performed twice, using two different relaxation delays (15 ms and 20 ms) for the extraction of the dipole-dipole cross-correlation rate. Hα(i)Cα(i)/HN(i)N(i) and Hα(i−1)Cα(i−1)/HN(i)N(i) dipole/dipole experiments are based on so-called quantitative Γ-spectroscopy and are of the HNCA and HNCOCA type. Experiments devised by the group of Bodenhausen were modified to refocus the passive $^{1,2}J_{NC\alpha}$ couplings. $^{3}J_{C'C'}$ values were taken from the literature (Hu and Bax, 1996). Data were processed and analyzed using the programs NMRPipe (Delaglio et al., 1995) and PIPP/CAPP (Garrett et al., 1991). Peak intensities were used to quantify cross-correlated relaxation rates. To facilitate peak picking procedures of the CSA/DD cross-correlation experiments (Yang et al., 1997, 1998; Yang and Kay, 1998; Kloiber and Konrat, 2000a) using NMRView software (Johnson and Blevins, 1994), in-house written scripts were devised to construct peak lists with frequency positions of the doublet components in the HNCO-type cross-correlation experiments. Peak lists were also generated automatically for the quantitative Γ-experiments on the basis of an HNCA ($C\alpha H\alpha(i)$-$NH^{N}(i)$) or ^{15}N-HSQC ($C\alpha H\alpha(i-1)$-$C\alpha H\alpha(i)$) assignments, respectively. HNCOCA-type DD/DD ($C\alpha H\alpha(i-1)/NH^{N}(i)$) cross-correlation experiments can either be analyzed as a 3D HNCO experiment (3D version, Figure 1B) or (in case of sufficient spectral resolution) as a conventional 2D ^{15}N-HSQC. The scripts are available from the authors upon request.

Experimental measurement of $\Gamma_{H\alpha(i)C\alpha(i),H(i)N(i)}$ *and* $\Gamma_{H\alpha(i-1)C\alpha(i-1),H(i)N(i)}$

The sequences for measuring $\Gamma_{H\alpha(i)C\alpha(i),HN(i)N(i)}$ (Figure 1A) and $\Gamma_{H\alpha(i-1)C\alpha(i-1),HN(i)N(i)}$ (Figure 1B) dipole-dipole cross-correlation rates are related to recently published sequences (Pelupessy et al., 1999a, 1999b) and are illustrated in Figure 1. The experiments for $\Gamma_{H\alpha(i)C\alpha(i),H(i)N(i)}$ and $\Gamma_{H\alpha(i-1)C\alpha(i-1),H(i)N(i)}$ are closely related to the sequences devised by Bodenhausen and co-workers (Pelupessy et al., 1999a, 1999b) in terms of the flow of magnetization. The sequence for $\Gamma_{H\alpha(i)C\alpha(i),H(i)N(i)}$ is based on an HNCA experiment (Kay et al., 1990), whereas $\Gamma_{H\alpha(i-1)C\alpha(i-1),H(i)N(i)}$ is obtained from an HNCOCA type experiment (Bax and Ikura, 1991). Details of the magnetization transfer can be found in the literature (Kay et al., 1990; Bax and Ikura, 1991; Pelupessy et al., 1999a,b). An important modification of the HNCOCA-type cross-correlation experiment, however, is that $^{13}C'$ chemical shift is recorded during t_1 (instead of $^{13}C^{\alpha}$) in a constant time manner ($2\tau_d$, Figure 1B). In what follows we focus on the modified ^{15}N-$^{13}C\alpha$ multiple-quantum evolution period during which the $^{13}C\alpha$-$^{1}H\alpha$ and ^{15}N-$^{1}H^N$ dipole interactions evolve. Figure 1 (shaded boxes) illustrates the pulse sequence element which is used in both sequences to quantify the relaxation interference. The simultaneous ^{13}C and ^{15}N 90° rf pulses create $2C_x^{\alpha}N_x$, which can be written as a sum of DQ and ZQ coherences. Two considerations are important. First, cross-correlation between $^{13}C\alpha$-$^{1}H\alpha$ and ^{15}N-$^{1}H^N$ dipole interactions must proceed for the complete relaxation period ($4T_C$). This is achieved by ensuring that the relative signs of the cross-correlation active dipolar Hamiltonians are not changed but preserved throughout the entire relaxation period. The simultaneous application of the amide $^{1}H^N$ selective and the $^{13}C\alpha$ inversion pulse in the middle of the relaxation period does not change the sign of the product of the two Hamiltonians and thus leaves the magnitude of the cross-correlation rate unchanged. Refocusing of ^{15}N chemical shift evolution during the $^{1}H^N$ inversion and $^{13}C\alpha$ refocusing pulses is achieved by the two 180° ^{15}N rf pulses and by accounting for the length of the $^{1}H^N$ and $^{13}C\alpha$ pulses in the relaxation delay; the second and third T_C element is reduced by the pulse length of the longer shaped pulse, either $^{1}H^N$ or $^{13}C\alpha$. In the present case, the following pulse lengths for the $^{1}H^N$ and $^{13}C\alpha$ selective pulses were used: $^{1}H^N$: RE-BURP (Geen and Freeman, 1991): 3.09 ms; $^{13}C\alpha$: RE-BURP (Geen and Freeman, 1991): 2.0 ms. The length of the two individual T_C elements were corrected accordingly to $T_C - 0.5^{*}pw_{180°}$ ($^{1}H^N$). $^{13}C\alpha$-$^{1}H\alpha$ and ^{15}N-$^{1}H^N$ dipole cross-correlations are active during both $^{1}H^N$ and $^{13}C\alpha$ selective pulses and only marginally reduced (Yang and Kay, 1998). No corrections for this effect were thus employed.

Secondly, $^{1,2}J_{NC\alpha}$ passive scalar couplings decrease the sensitivity of the experiment due to the build-up of unwanted anti-phase magnetizations (e.g., $4C_x^{\alpha}N_yN_z$, $4C_x^{\alpha}N_yC_z^{\alpha}$, $8C_y^{\alpha}N_yC_z^{\alpha}N_z$). As can be seen from Figure 1, this effect is suppressed through the application of the $^{13}C\alpha$ selective refocusing pulse in the middle of the relaxation period. Additionally, evolution under the homonuclear $^{1}J_{C\alpha C\beta}$ is suppressed by the refocusing pulse. It is thus not necessary to adjust the relaxation period to $4T_C = = 1/^{1}J_{C\alpha C\beta}$. Although the signal intensities of residues for which $^{13}C\beta$ shifts are within the bandwidth of the RE-BURP pulse (e.g., Ser, Thr or Leu residues, respectively) are reduced, the extracted cross-correlation rates are not affected. Typical experimental results obtained on ^{13}C,^{15}N-labeled ubiquitin are shown in Figure 2. Due to the good spectral resolution in the ^{15}N-^{1}H HSQC of ubiquitin a 2D version of the HNCOCA sequence of Figure 1B was recorded (by omitting the $^{13}C'$ indirect evolution period t_1).

To obtain $\Gamma_{H\alpha(i)C\alpha(i),H(i)N(i)}$ and $\Gamma_{H\alpha(i-1)C\alpha(i-1),H(i)N(i)}$ cross-correlation rates, two sets of complementary experiments were recorded, as described previously (Pelupessy et al., 1999a,b). The dipole-dipole cross-correlation leads to a partial conversion of $2C_x^{\alpha}N_x$ into $8C_y^{\alpha}H_z^{\alpha}N_yH_z^N$ (Chiarparin et al., 1999). In experiment I, the signal intensity is proportional to the expectation value of the two-spin coherence $2C_x^{\alpha}N_x$, (selected by phase = y of the rf pulses at time point a in the sequence), whereas in experiment II signal arising from cross-correlation, $8C_y^{\alpha}H_z^{\alpha}N_yH_z^N$, are recorded (at time point a: phase = x). In experiment I, evolution due to $^{1}J_{CH}$ is refocused (omitting the ^{1}H 180° shown in brackets in Figure 1, the phase of ^{13}C,^{15}N, at time point b being = x), whereas $^{1}J_{NH}$ evolves during the constant time period T_N (where the ^{15}N chemical shift is recorded) for the time $2\xi = 1/(2J_{NH})$ (Figure 1). In the second experiment II, the coherence $8C_y^{\alpha}H_z^{\alpha}N_yH_z^N$ is selected. This is achieved by applying the ^{1}H 180° (the scalar coupling evolves for the time $2\zeta = 1/2J_{CH}$), setting the phase of ^{13}C and ^{15}N rf pulses (at time point b) to y, and by adjusting the delay $\xi = 0$. The cross-correlation rates can be obtained from the ratio of the

Table 1 Parameters in cross-correlation spectra (ubiquitin)

Experiment	Data matrix	Relaxation delay	Experimental time
$\Gamma_{H\alpha(i)C\alpha(i),H(i)N(i)}$	25×22×512	15 ms	43 h
$\Gamma_{H\alpha(i-1)C\alpha(i-1),H(i)N(i)}$	2D:32×512)[a] / 3D:13×25×512	15 ms	1.6 h/20 h
$\Gamma_{C'(i-1),H\alpha(i)C\alpha(i)}$	25×25×512	26 ms	48 h
$\Gamma_{C'(i-1),H\alpha(i-1)C\alpha(i-1)}$	25×25×512	26 ms	48 h
$\Gamma_{H\alpha(i-1)C\alpha(i-1),H\alpha(i)C\alpha(i)}$	2D:32×512	15 ms and 20 ms[b]	1.6 h/20 h

[a]In the 2D version of the experiment, 80 and 1024 scans were used for the reference and cross experiment, respectively.
[b]Average cross-correlation rates were used.

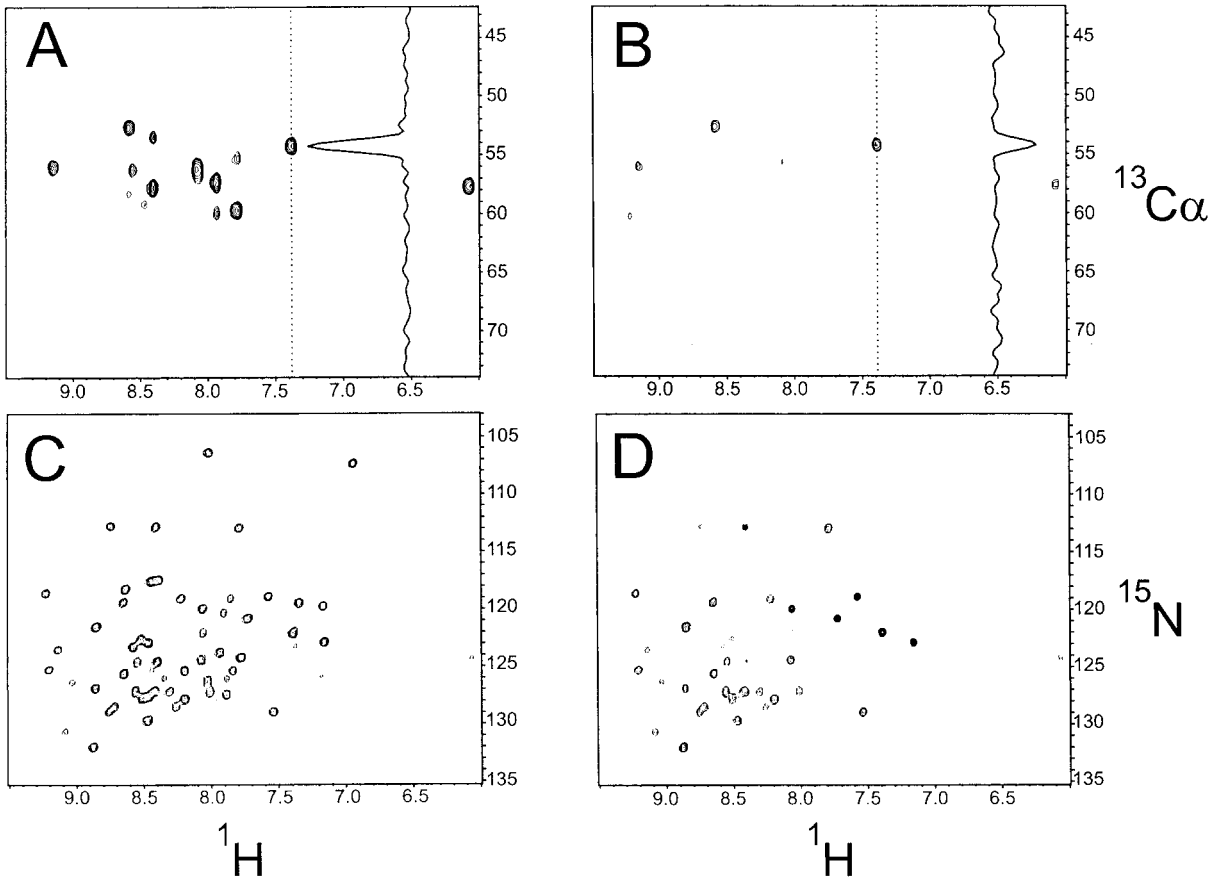

Figure 2. Experimental results for $^{13}C,^{15}N$-labeled ubiquitin using the sequences of Figure 1. (A,B) F_1-F_3 cross sections through the 3D spectra (Figure 1A) at selected ^{15}N chemical shifts. The 2D planes selected at the ^{15}N frequency, F_2 = 125.1 ppm, in (A) and (B) correspond to the reference and cross experiment, respectively. F_1 slices through the cross peak indicated with the dotted line illustrate the achieved S/N ratio of the data set. (C,D) Representative regions of the 2D HNCOCA cross-correlation experiment (Figure 1B) for measuring $\Gamma_{H\alpha(i-1)C\alpha(i-1),H(i)N(i)}$ (recorded by omitting the $^{13}C'$ indirect evolution time t_1), (C) reference and (D) cross experiment (negative cross peaks are shown in bold). Experimental parameters are given in the legend of Figure 1 and Table 2.

signal intensities in the two experiments as described below (Pelupessy et al., 1999; Chiarparin et al., 1999, 2000). For the measurement of $\Gamma_{H\alpha(i)C\alpha(i),HN(i)N(i)}$ and $\Gamma_{H\alpha(i-1)C\alpha(i-1),HN(i)N(i)}$, data sets with T_C of 15 ms were recorded. It should be noted that differential amide proton T_1 relaxation and intermolecular exchange between amide protons and water molecules in experiments I and II lead to a slight reduction of signal intensities in the cross-correlation experiment (II). These effects were estimated to reduce the observed signal intensities in the cross-correlation experiment II by about 15%. In order to ensure that this signal reduction does not spoil the accuracy of the extracted dihedral angles, numerical analysis have been performed for reduction levels of 10, 15 and 20%, respectively. No significant changes (less than 5°) in extracted dihedral angles were observed, thus corroborating the reliability of the approach. However, differential intermolecular exchange in experiments I and II can be avoided by adding a ^{1}H 180° pulse at time point a in the sequence of experiment I, and a 180° phase shift of the ^{1}H 90° pulse after the ^{15}N chemical shift evolution T_N in both experiments (I and II). Experimental parameters used to record cross-correlation spectra and a list of experimentally obtained S/N values are given in Tables 1 and 2. Figure 3 demonstrates the correlation between experimental cross-correlation rates and calculated values based on the crystal structure (Vijay-Kumar et al., 1987).

Error analysis of individual rates for ubiquitin

Error propagation was obtained from a Monte Carlo error analysis (Kamath and Shriver, 1989; Palmer, et al., 1991) and has been described elsewhere (Kloiber and Konrat, 2000a). To this purpose, a Gaussian distribution of peak intensities was assumed, centered at the measured value with the root-mean-square base-line noise (estimated by NMRPipe) as standard deviation of the distribution. Typically, 1000 simulated data sets were chosen at random from these distributions to extract cross-correlation rates and errors.

Generation of the dihedral angle probability surface (Z-surface)

The *Z*-surface has been defined as the probability of a certain experimental parameter Γ to result from a particular set of backbone dihedral angles φ and ψ. The Z-surface was generated following the strategy described by Oldfield and co-workers (Le et al., 1995). Z_i for a specific cross-correlation rate is defined as

$$Z_i = \exp\{-\Delta\Gamma_i^2(1 - P_i)\}, \quad (1a)$$

$$P_i = \exp\{-[\Delta\Gamma_i^2/(2\sigma_i^2)]\} \quad (1b)$$

where $\Delta\Gamma_i$ is the difference between experimental and calculated rate. To include experimental errors, the square difference is weighed with a factor proportional to a Gaussian probability P_i; σ_i is the associated experimental error of the rate Γ_i (which corresponds to the uncertainty in the deviation). As a consequence, data with large errors contribute a smaller penalty to the fit. As an additional spectral parameter we included the homonuclear $^3J_{C'C'}$ scalar coupling constant (Hu and Bax, 1996). This parameter turned out to be of crucial importance to unambiguously identify backbone dihedral angles in the β-sheet region of Ramachandran space (see below). The total Z surface is obtained by taking the product of the individual cross-correlation probabilities, $Z=Z_1Z_2Z_3...Z_N$, where N is the number of available experimental parameters. Table 3 lists the experimental parameters which were used in the construction of the Z-surface. Note that $\Gamma_{H\alpha(i-1)C\alpha(i-1),H\alpha(i)C\alpha(i)}$ probes the pseudodihedral angle Σ which is defined by two planes subtended by the atoms {α(i−1), Cα(i−1), Hα(i) and Cα(i)} and which is in turn related to the backbone dihedral angles as $\Sigma = \psi(i-1) + \varphi(i)$ (Chiarparin et al., 2000). The Z-surface is thus defined as the φ(i),ψ(i−1)-probability of the observed experimental parameters. A similar graphical construction was recently used to resolve contradictions from overdetermined NMR cross-correlation rates (Tolman et al., 2000). To better illustrate the strategy, a hypothetical construction of a protein Z-surface using the spectral parameters of Table 3 is shown in Figure 4. Whereas a single experimental parameter is consistent with a multitude of solutions (Figure 4A), multiplication with the Z-surfaces of additional experimental parameters reduces the set of solutions to a single pair of φ(i),ψ(i−1) values (Figure 4B-4E).

The theoretical cross-correlation rates in Equation 1 were calculated assuming the slow-motion limit (neglecting high-frequency $J(\omega_C)$ components).

CSA-DD cross correlation rates $\Gamma_{C',H\alpha C\alpha}$ are related to the dihedral angle by the analytical expression (Goldman, 1984):

$$\Gamma_{C',H\alpha C\alpha} = (4/15)(h/2\pi)\omega_C\gamma_C\gamma_H(r_{CH})^{-3}\tau_C(f_X + f_Y + f_Z), \quad (2)$$

Table 2. Average signal-to-noise ratios of the dipole-dipole and CSA-dipole cross-correlation experiments obtained on $^{13}C,^{15}N$-labeled ubiquitin

Experiment	Ubiquitin	Pulse sequence
$\Gamma_{H\alpha(i)C\alpha(i),H(i)N(i)}$[a]	10 ± 7.6/102 ± 49	Figure 1A
$\Gamma_{H\alpha(i-1)C\alpha(i-1),H(i)N(i)}$[a]	4.5 ± 3.0/50 ± 14	Figure 1B
$\Gamma_{C'(i-1),H\alpha(i)C\alpha(i)}$[b,c]	45 ± 19/41 ± 17	Kloiber and Konrat, 2000a
$\Gamma_{C'(i-1),H\alpha(i-1)C\alpha(i-1)}$[b]	68 ± 24/62 ± 2	Yang et al., 1998
$\Gamma_{H\alpha(i-1)C\alpha(i-1),H\alpha(i)C\alpha(i)}$[a]	11 ± 10/42 ± 22	Chiarparin et al., 2000

[a]Two S/N values corresponding to the cross-order reference experiments are given.
[b]Two S/N values corresponding to the two multiplet components are given.
[c]The average S/N value of the reference experiment were as follows: Ubiquitin: 52 ± 21 (intra-residue)/ 22 ± 5 (inter-residue) (Kloiber and Konrat, 2000a).

Table 3. Experimental parameters used for the construction of the Z-surface for Ubiquitin

Parameter	Angle	Experiment
$\Gamma_{H\alpha(i)C\alpha(i),H(i)N(i)}$	$\varphi(i)$	Figure 1A
$\Gamma_{H\alpha(i-1)C\alpha(i-1),H(i)N(i)}$	$\psi(i-1)$	Figure 1B
$\Gamma_{C'(i-1),H\alpha(i)C\alpha(i)}$	$\varphi(i)$	Kloiber and Konrat, 2000a
$\Gamma_{C'(i-1),H\alpha(i-1)C\alpha(i-1)}$	$\psi(i-1)$	Yang et al., 1998
$\Gamma_{H\alpha(i-1)C\alpha(i-1),H\alpha(i)C\alpha(i)}$	$\{\psi(i-1), \varphi(i)\}$	Chiarparin et al., 2000
$^3J_{C'C'}$	$\varphi(i)$	Hu and Bax, 1996

where γ_i is the gyromagnetic ratio of nucleus i, $\omega_C = \gamma_C B_0$, r_{CH} is the $C^\alpha H^\alpha$ bond length (set to 1.09 Å), τ_C is the correlation time describing the overall tumbling of the assumed rigid and isotropically tumbling molecule, and the factors f_i are projections of the dipolar vector onto the principal components of the carbonyl CSA tensor, $\frac{1}{2}(3\cos^2\theta_i - 1)$. The angles θ_i are related to the dihedral angle φ and ψ in the following way (Yang et al., 1997; Kloiber and Konrat, 2000a):

$$\cos\theta_x = -0.3095 + 0.3531\cos(\varphi + D), \quad (3a)$$

$$\cos\theta_y = -0.1250 - 0.8740\cos(\varphi + D), \quad (3b)$$

$$\cos\theta_z = -0.9426\sin(\varphi + D), \quad (3c)$$

D is $-120°$ in case of $\Gamma_{C'(i-1),H\alpha C\alpha(i-1)}$ and $120°$ in case of $\Gamma_{C'(i-1),H\alpha C\alpha(i)}$ for non-glycine residues. If glycine is involved, the rates are the sums of both expressions ($D = -120°$ and $+120°$). In the calculation values of 244, 178 and 90 ppm were employed for σ_{xx}, σ_{yy} and σ_{zz}, with x and y axes located in the peptide plane and the y axis of the CSA tensor rotated by 8° with respect to the carbonyl bond (Teng et al., 1992).

Dipole-dipole cross-correlation rates $\Gamma_{H\alpha C\alpha,HN}$ were calculated according to

$$\Gamma_{H\alpha C\alpha,HN} = (2/5)(h/2\pi)^2\gamma_C\gamma_N\gamma_H^2(r_{CH})^{-3}(r_{NH})^{-3}\tau_C(3\cos^2\theta - 1)/2, \quad (4)$$

where the symbols have their ususal meaning, r_{NH} is the NH bond length (set to 1.0 Å). The projection angles θ in the two experiments are related to the backbone dihedral angles φ and ψ (Reif et al., 1997; Pelupessy et al., 1999a) according to

$$\cos(\theta) = 0.163 + 0.819\cos(\psi - 120°,) \quad (5a)$$

$$\cos(\theta) = 0.163 - 0.819\cos(\varphi - 60°), \quad (5b)$$

where planar peptide bond geometry and a trans configuration has been assumed. The dipole-dipole cross-correlation rate $\Gamma_{H\alpha(i-1)C\alpha(i-1),H\alpha(i)C\alpha(i)}$ is given by

$$\Gamma_{H\alpha(i-1)C\alpha(i-1),H\alpha(i)C\alpha(i)} = (2/5)(h/2\pi)^2\gamma_C^2\gamma_H^2(r_{CH})^{-6}\tau_C(3\cos^2\theta - 1)/2 \quad (6)$$

where θ is the angle subtended between successive Cα-Hα vectors $\cos\theta$ is related to angles $\Psi(i-1)$ and $\varphi(i)$ by (Chiarparin et al., 2000)

$$\cos(\theta) = -0.106 + 0.894\cos(\psi(i-1) + \varphi(i) - 180°). \quad (7)$$

Equations 2–7 can be rearranged to Karplus relations of the usual form (Sprangers et al., 2000)

$$\Gamma = A\ \cos^2(\alpha) + B\ \cos(\alpha) + C, \quad (8)$$

Karplus relations were used to calculate theoretical rates encountered in the generation of Z-surfaces as a function of dihedral angles $\varphi(i)$ and $\Psi(i-1)$. The Karplus parameters for cross-correlation rates and the $^3J_{C'(i)C'(i+1)}$ scalar coupling constants are summarized in Table 4.

Extraction of experimental cross-correlation rates is based on the following relationships:

$$\Gamma_{CSA/DD} = 1/(2T_C)\ln(I_{df}/I_{uf})/S^2, \quad (9a)$$

$$\Gamma_{DD/DD} = 1/(2T_C)\tanh^{-1}(I_{cross}/I_{ref})/S^2, \quad (9b)$$

$$^3J_{C'(i)C'(i+1)} = 1/(2\pi T_C)\tan^{-1}\sqrt{(-I_{cross}/I_{ref})} \quad (9c)$$

where I_{uf}/I_{df} are the upfield/downfield components of the resolved multiplett lines and I_{cross}/I_{ref} refer to the complementary data sets in the quantitative Γ-experiments. T_c is the respective constant time delay. To account to some extent for internal dynamics, experimental rates have been scaled with the ^{15}N order parameter S^2 (Tjandra et al. 1995) which has been assumed to be representative for ps to ns motion of the entire peptide plane.

Note that the extraction of experimental rates $\Gamma_{C'(i-1),H\alpha(i)C\alpha(i)}$ (associated with the angle φ is somewhat more complicated, since the experiment involves simultaneous excitation of coherences $2C'_x(i-1)C^\alpha_x(i-1)$ and $2C'_x(i-1)C^\alpha_x(i)$ which depend on $\Psi(i-1)$ and $\varphi(i)$, respectively. In order to discern the contributions, a reference experiment has to be recorded to determine effective transfer efficiencies to the intra- and interesidue Cα atoms that are determined by differences in scalar coupling between ^{15}N and $^{13}C\alpha$ and different transverse relaxation times of Cα. The exact description of the experiment and extraction procedure can be found elsewhere (Kloiber and Konrat, 2000). Intensities for scalar coupling constants were back-calculated from the published rates (Hu and Bax, 1996) assuming $T_C = 40$ ms and an estimated noise level of 1% with respect to the reference peak in the 2D quantitative J-experiment.

Z-surfaces were calculated in a $\Psi(i-1)/\varphi(i)$ space on a per-residues basis, and positions and heights of maxima in Z were subsequently evaluated. The uniqueness of a solution was determined discarding maxima lower than 95% of the height of the absolute maximum and subjecting remaining maxima to an analytical error analysis. Differentiation of Z (in this case the deviations were not weighted with the factor $(1 - P_i)$) with respect to the uncertainty in the deviations $\Delta\Gamma_i$ in each experiment yields

$$\partial \ln Z = 2\Sigma_i \Delta\Gamma_i \partial \Delta\Gamma_i \quad (10)$$

with i ranging over the six experiments. Since all parameters are defined for each point of the surface (the uncertainty in the deviations is equal to the

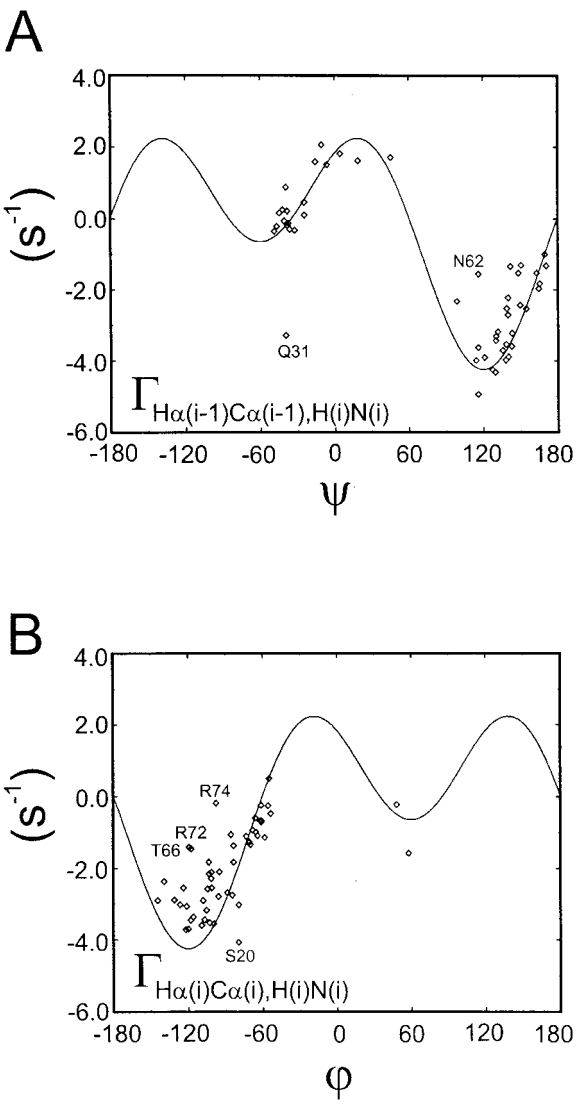

Figure 3. Correlation between calculated and experimental values of (A) $\Gamma_{H\alpha(i-1)C\alpha(i-1),H(i)N(i)}$ and (B) $\Gamma_{H\alpha(i)C\alpha(i),H(i)N(i)}$ for non-glycine residues in ubiquitin (Vijay-Kumar et al., 1987; Wand et al., 1996). For the calculation (using Equations 5a and 5b) standard bond lengths and angles ($r_{NH} = 1.00$ Å and $r_{CH} = 1.09$ Å) were used. $\Gamma_{H\alpha(i)C\alpha(i),H(i)N(i)}$ and $\Gamma_{H\alpha(i-1)C\alpha(i-1),H(i)N(i)}$ dipole/dipole cross-correlation experiments were recorded using the pulse sequences of Figures 1A and 1B. Outliers are labeled according to their residue position.

Table 4. Karplus parameters for cross-correlated spin relaxation rates and homonuclear $^3J_{C'C'}$ scalar coupling constants

Experiment	A	B	C	D
$\Gamma_{H\alpha(i)C\alpha(i),H(i)N(i)}$	1.006	−0.4005	−0.4601	−60
$\Gamma_{H\alpha(i-1)C\alpha(i-1),H(i)N(i)}$	1.006	0.4005	−0.4601	−120
$\Gamma_{C'(i-1),H\alpha(i)C\alpha(i)}$	129.64	−21.66	−96.82	120
$\Gamma_{C'(i-1),H\alpha(i-1)C\alpha(i-1)}$	129.64	−21.66	−96.82	−120
$\Gamma_{H\alpha(i-1)C\alpha(i-1),H\alpha(i)C\alpha(i)}$	1.199	−0.824	−0.483	180
$^3J_{C'C'}$	1.33	−0.88	0.62	0

experimental error σ_i), the error in Z can be determined for the two highest maxima and subsequently be compared to the difference in their Z values; the highest maximum was assumed to be unique in case the difference in Z values exceeded the sum of their respective errors. Errors in extracted angles were calculated based on a Monte Carlo analysis that was carried out simultaneously for all intensities involved in finding one dihedral angle pair. In analogy to the error analysis in the individual experiments, intensities were varied in a range ± 4 times the root-mean-square baseline noises of the pertinent experiment and weighted by their Gaussian probability. This procedure is time-consuming in that a Z-surface has to be generated for each initial condition. Therefore, representative residues Lys6 (β-sheet) and Ala28 (α-helix) were chosen in order to investigate the influence of experimental errors in regions of well-defined secondary structure. The resulting standard deviation in angles (φ/Ψ) after 2000 repeats amounted to about (2.5°/3.1°) for residue Lys6 and about (0.6°/1.9°) for residue 28 (see also Table 5). These surprisingly small values are presumably due to the fact that the simultaneous random variations of all intensities result in a partial compensation of deviations.

Automated analysis and extraction of dihedral angles

A Matlab-based program was developed to automatically derive backbone dihedral angles from experimental data. The program computes experimental rates on the basis of cross peak intensities, experimental errors on the basis of intensities and the root mean square noise as estimated by the program NMRPipe, and theoretical rates on the basis of Karplus equations for grid points of specified resolution of 1° on the φ(i)/Ψ(i−1) surface. The program has been implemented on UNIX platforms and is available from the authors upon request.

Table 5. Deviations in angles for two representative residues in ubiquitin: deviations in the individual experiments and deviations according to the Z-surface analysis. The precision of the obtained angles are estimated from a Monte Carlo error analysis

Parameter	Thr7 (°)	Ala28 (°)
$\Gamma_{H\alpha(i)C\alpha(i),H(i)N(i)}$	13.8	0.3
$\Gamma_{H\alpha(i-1)C\alpha(i-1),H(i)N(i)}$	6.7	1.2
$\Gamma_{C'(i-1),H\alpha(i)C\alpha(i)}$	10.0	5.5
$\Gamma_{C'(i-1),H\alpha(i-1)C\alpha(i-1)}$	0.4	1.4
$\Gamma_{H\alpha(i-1)C\alpha(i-1),H\alpha(i)C\alpha(i)}$	50.7	3.9
$^3J_{C'C'}$	13.6	8.5
Z-surface (φ)	4.2	0.1
Z-surface (Ψ)	4.8	2.0
Error analysis (φ)[a]	2.5	0.6
Error analysis (Ψ)[a]	3.1	1.9

[a]Error propagation was obtained from a Monte Carlo error analysis (see Materials and methods).

Results and discussion

The proposed sequences for $\Gamma_{H\alpha(i-1)C\alpha(i-1),N(i)HN(i)}$ and $\Gamma_{H\alpha(i)C\alpha(i),N(i)HN(i)}$ (Figure 1) provide good signal-to-noise, notably by refocusing the passive $^{1,2}J_{NC\alpha}$ couplings. Figure 3 illustrates the correlation between measured $\Gamma_{H\alpha(i-1)C\alpha(i-1),H(i)N(i)}$ (A) and $\Gamma_{H\alpha(i)C\alpha(i),H(i)N(i)}$ (B) values for non-glycine residues in ubiquitin using the pulse scheme of Figure 1. The values of φ and ψ were taken from the X-ray-derived structure (Vijay-Kumar et al., 1987). A correlation time of 4.2 ns was used. On average, the correlations between predicted and measured $\Gamma_{H\alpha(i)C\alpha(i),H(i)N(i)}$ and $\Gamma_{H\alpha(i-1)C\alpha(i-1),H(i)N(i)}$ values are quite good and comparable to the previously published sequences by Bodenhausen and co-workers (Pelupessy et al., 1999; Chiarparin et al., 1999, 2000). Some deviations between predicted and NMR-derived values were observed for residues: Thr14, Thr22, Gln31, Asp52,

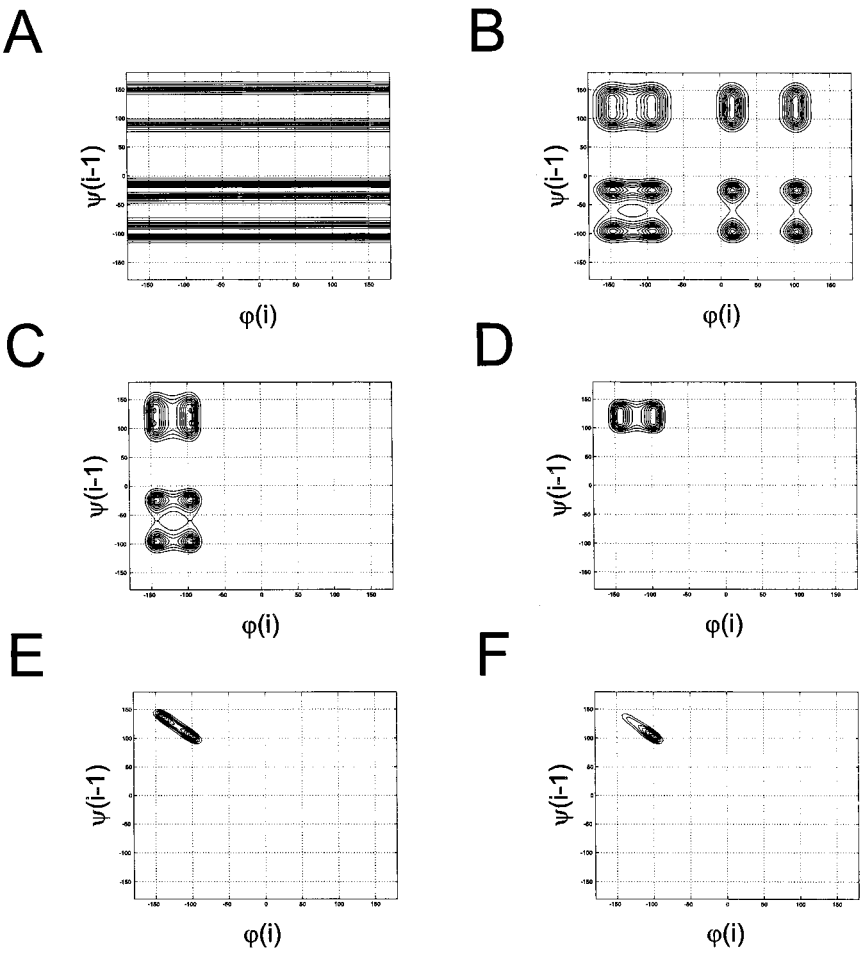

Figure 4. Schematic description of the generation of the dihedral angle probability surface, *Z-Surface.* The cross-correlation rates are defined as follows: $\Gamma_1(\psi)$ = CSA/dipole $\Gamma_{C'(i),C\alpha(i)H\alpha(i)}$; $\Gamma_2(\varphi)$ = CSA/dipole $\Gamma_{C'(i-1),C\alpha(i)H\alpha(i)}$; $\Gamma_3(\varphi)$ = dipole/dipole $\Gamma_{C\alpha(i)H\alpha(i),N(i)H(i)}$; $\Gamma_4(\psi)$ = dipole/dipole $\Gamma_{C\alpha(i-1)H\alpha(i-1),N(i)H(i)}$; $\Gamma_5(\varphi,\psi)$ = dipole/dipole $\Gamma_{C\alpha(i-1)H\alpha(i-1),C\alpha(i)H\alpha(i)}$; (A) ${}^1Z\{\Gamma_1(\psi)\}$; (B) ${}^2Z\{\Gamma_1(\psi)\Gamma_2(\varphi)\}$; (C) ${}^3Z\{\Gamma_1(\psi)\Gamma_2(\varphi)\Gamma_3(\varphi)\}$; (D) ${}^4Z\{\Gamma_1(\psi)\Gamma_2(\varphi)\Gamma_3(\varphi)\Gamma_4(\psi)\}$; (E) ${}^5Z\{\Gamma_1(\psi)\Gamma_2(\varphi)\Gamma_3(\varphi)\Gamma_4(\psi)\Gamma_5(\varphi,\psi)\}$; (F) ${}^6Z\{\Gamma_1(\psi)\Gamma_2(\varphi)\Gamma_3(\varphi)\Gamma_4(\psi)\Gamma_5(\varphi,\psi){}^3J_{C'C'}(\varphi)\}$. Hypothetical dipole/dipole and CSA/dipole cross-correlation rates were computed for a dihedral angle pair $\varphi(i),\psi(i-1) = -100°, 100°$. The ${}^3J_{C'C'}$ scalar coupling constant was calculated using the empirical Karplus relation (Hu and Bax, 1996). In the calculation standard bond lengths (r_{NH} = 1.00 Å and r_{CH} = 1.09 Å) and angles, planar peptide bond geometry, and uniform values for both the components of the ${}^{13}C'$ CSA tensor and the orientation of the tensor with respect to the molecular peptide frame were assumed (Teng et al., 1992). The correlation time τ_C was 4.2 ns.

Asn62, and Arg74 {Ψ(i−1)}, and Thr9, Ser20, Glu34, Leu43, Asn62, Thr66, Arg72, and Arg74 {φ(i)}, the most significant outliers are labeled in Figure 3. Some of these residues were identified as flexible, as established by ^{15}N relaxation (Thr9 has an order parameter of 0.73 and a lower than average NOE; Ser20 has a slightly lowered NOE of 0.66, Asn62 has an NOE of 0.6 and an order parameter of 0.70, Leu73 with an NOE of 0.35 and an order parameter of 0.56, and Arg74 exhibiting an NOE of almost zero; T_1/T_2 ratio for Arg74 is lower than average, i.e., 1.62, the average value being 2.69 ± 0.33) (Tjandra et al. 1995), or $^{13}C^{\alpha}$-$^{1}H^{\alpha}$ transverse relaxation (Ile13, Glu34, Ile61, Arg72, Leu73, Arg74) (Wand et al. 1996) (note that dynamics of the $C^{\alpha}H^{\alpha}$ vector of residue i−1 affects the rate of residue i in case of $\Gamma_{H\alpha(i-1)C\alpha(i-1),H(i)N(i))}$, others exhibited low signal/noise ratios (Thr9, Asp21, Leu43, Arg74 in $\Gamma_{H\alpha(i)C\alpha(i),H(i)N(i))}$. Neither evidence for dynamics nor low S/N have been found for (Thr22/Asp21), (Gln31/Ile30), (Asp52/Glu51) and (Thr66/Ser65). ^{15}N relaxation data are missing for Arg72, Gln31 and Ile13, and $^{13}C\alpha$ relaxation data are

missing for Ser20, Asp21, Glu51 and Asp58. However, Cα relaxation for Ile30 indicates an internal correlation time of > 1 ns, which could eventually indicate that the extracted order parameter of 0.93 may be unreliable.

Surfaces shown in Figure 4 are hypothetical and simply illustrate the construction of the Z-surface based on cross-correlation rates and $^3J_{C'C'}$ scalar coupling constants. It shows the decrease in multiplicity of solutions as a larger number of experiments is employed. Note that by the use of the five cross-correlated relaxation experiments alone, it is impossible to resolve the residual two-fold degeneracy of solutions that are due to the similar symmetry properties of the interactions with respect to the dihedral angles. The $^3J_{C'(i)C'(i+1)}$ coupling constant is symmetric around $\varphi = 0°$ rather than $\varphi = 120°$ and is crucial for ruling out residual φ ambiguities. Typical examples of experimental data obtained on ubiquitin are shown in Figure 5. In this case, five experimental cross-correlation rates (see Materials and methods) and the $^3J_{C'C'}$ scalar coupling constant were used to construct the Z-surfaces as outlined in Equation 1. Peptide planes Thr7/Lys6 and Ala28/Lys27 were taken as representative examples for β-sheet or α-helical secondary structure elements. The procedure was performed on a per-residue basis in ubiquitin. The N-terminal, C-terminal residues, prolines, glycines, and residues following a glycine in the sequence have been excluded from the analysis, and residues Glu16 and Glu24 have not been assigned, so that the final set comprised 60 residues. However, not all residues gave a complete set of experimental data. The two data sets for $\Gamma_{H\alpha(i-1)C\alpha(i-1),H\alpha(i)C\alpha(i)}$ involving different relaxation delays were complementary to some extent as to which resonances could be observed. Thus, both sets have been combined, taking into account residues with available data in either of the two experiments. A complete set of experimental data was thus obtained for 31 residues (51.7%), for 18 residues (30.5%) one experiment was missing, and 6 residues (10.0%) provided only 4 experiments. For 5 residues (8.3%) less than 4 experiments could be obtained. In the following we list the percentages of completeness for the five individual cross-correlation and the ^3J scalar coupling experiments (refering to the 60 analyzed residues): CSA/DD (ψ) (Yang et al., 1997, 1998; Yang and Kay, 1998): 96.6% (58); CSA/DD (φ) (Kloiber and Konrat, 2000a): 75.0% (45); DD/DD (ψ) (Pelupessy et al., 1999): 81.7% (49); DD/DD (φ) (Chiarparin et al., 1999): 86.7% (52); DD/DD (Σ) (Chiarparin et al., 2000): 98.3% (59 residues; 51 and 58 for the experiments with 15 ms and 20 ms, respectively); $^3J_{C'C'}$ (φ) (Hu et al. 1995): 88.3% (53). 96.8% of the residues with a complete data set revealed a unique solution. For 72.2% of the residues with only 5 experiments available, a unique pair of (φ(i),ψ(i−1)) values could be obtained. Of residues for which only 4 experiments were available only one did reveal a unique solution (16.7%). Thus, the total number of residues for which a unique solution was obtained is 44 which corresponds to 73.3% of the residues of the data set (60 residues). For 21 residues (26.7%), ambiguous although not necessarily wrong φ(i),ψ(i−1)) values were obtained. Of course, the most obvious cause for non-unique solutions is the incompleteness of the data set. Residues with 5 experiments have a second solution in 5 of 18 cases. The question of whether the solution can be found in these cases is strongly dependent on the type of experiment missing. Naturally, if the coupling constant or $\Gamma_{H\alpha(i-1)C\alpha(i-1),H\alpha(i)C\alpha(i)}$ is not available, there is no possibility of resolving all ambiguities. However, there are cases where $\Gamma_{C'(i-1),H\alpha(i)C\alpha(i)}$ is missing; this rate is, in some cases, not necessary to get a single solution, since $\Gamma_{H\alpha(i)C\alpha(i),N(i)HN(i)}$ provides the means to distinguish negative from positive φ angles for certain ranges, and the coupling constant shows no degeneracy between $\varphi = -180°$ and approximately $-100°$. Therefore, solutions can be found for residues in extended conformation, even if $\Gamma_{C'(i-1),H\alpha(i)C\alpha(i)}$ is missing (e.g., Arg42-Phe45). However, the better sensitivity of the $\Gamma_{C'(i-1),H\alpha(i)C\alpha(i)}$ compared to the $\Gamma_{H\alpha(i)C\alpha(i),N(i)HN(i)}$ experiment confers the advantage of higher accuracy. On the other hand, in α-helices, it might be sufficient to have only one experiment for Ψ since in case of only twofold degeneracy $\{\Gamma_{C'(i-1),H\alpha(i-1)C\alpha(i-1)}\}$, $\Gamma_{H\alpha(i-1)C\alpha(i-1),H\alpha(i)C\alpha(i)}$ is sufficient to discern the two solutions. In some rare cases, residual ambiguities are due to symmetry, although a complete data set is available. Given that a set of distinct solutions is provided by the procedure (be it for reasons of symmetry or lack of data), one could think of using additional information such as provided by the chemical shift data base TALOS (Cornilescu et al., 1999) to distinguish between the solutions. Using this approach, residual ambiguities could be resolved for additional residues Gln2, Ser20, Ile23, Asn25, Lys29, Glu34, Tyr59 and Gln60.

Figure 6 illustrates the correlation between NMR (Cornilescu et al., 1998) and X-ray-derived φ and ψ values for ubiquitin (Vijay-Kumar et al., 1987). The

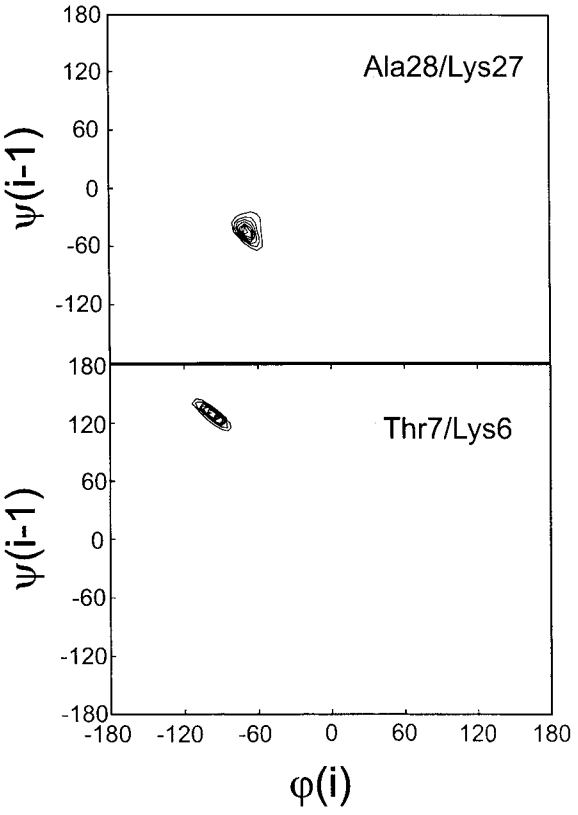

Figure 5. Experimental Z-surface plots, ${}^{6}Z\{\Gamma_1(\psi)\Gamma_2(\varphi)\Gamma_3(\varphi)\Gamma_4(\psi)\Gamma_5(\varphi,\psi)\ \Gamma_6(\varphi)\}$, for Thr7/Lys6 (β-sheet) and Ala28/Lys27 (α-helix) in ubiquitin. Calculation parameters were identical to Figure 4.

following residues yielded solutions deviating from the x-ray structure: Phe4 and Glu18 (yielded symmetry related dihedral angles which could not be resolved), Thr14 (low S/N in $\Gamma_{H\alpha(i-1)C\alpha(i-1),H\alpha(i)C\alpha(i)}$), Asp21 (low S/N in $\Gamma_{H\alpha(i-1)C\alpha(i-1),H\alpha(i)C\alpha(i)}$ experiment), Gln31 (with a rate $\Gamma_{H\alpha(i-1)C\alpha(i-1),N(i)HN(i)}$ that is typical for a positive Ψ value, although the residue is located in an α-helix). Residue Glu51 comes out right using $\Gamma_{H\alpha(i-1)C\alpha(i-1),H\alpha(i)C\alpha(i)}$ recorded with a delay of 20 ms; this residue as well as Asp58 do not show strongly deviating rates but give, due to the lack of one experimental data set each, two similar solutions. Residues Thr9 and Arg74 yield wrong solutions but are located in a loop region and at the C-terminus of the protein, respectively. Note that outliers mainly concern the angle Ψ(i−1), since the procedure shows a bias towards the determination of φ(i) (4 vs 3 experiments). We assume that the observed deviations are due to significant intramolecular dynamics at these sites. For example, the peptide plane Thr9/Leu8 is located in a loop connecting strand β1 and β2; Asp21/Ser20 is within a loop between β2 and the α-helix, Gln31/Ile30 is located towards the C-terminus of the α-helix (in the X-Ray structure the helix extends till Glu34), Glu51/Leu50 is at the end of β5, Asp58/Ser57 is within the 3_{10} helix, and Arg74/Leu73 is close to the C-terminus of the polypetide chain (76 residues). The most interesting outliers, however, are the peptide planes Phe4/Ile3 and Thr14/Ile13 which are located in strands β1 and β2 and are connected via inter-strand hydrogen bonds (HN{I3}-CO{L15}; HN{V5}-CO{I13}, Cordier and Grzesiek, 1999), indicating that the observed deviations reflect correlated motion in this β-sheet. Most importantly, in an independent study Bodenhausen and co-workers (Tolman et al., 2000) have shown that inconsistencies between dihedral angles derived from four complementary cross-correlation rates for Phe4 and Val5 can be resolved by assuming a model in which the peptide plane spanned by the Val5/Phe4 jumps through 40° between two sites.

The pairwise root-mean-squared differences (calculated disregarding the above-mentioned outliers) for (φ/Ψ) are (14.44°/14.18°) and (14.41°/12.00°) for angles derived from the X-ray structure and the NMR ensemble, respectively. The observed rmsd values compare favorably with the pairwise rmsd values obtained from an analysis of the backbone angles in the single experiments: using only residues that gave unique solutions (outliers excluded), rmsd values (and number of observations) were: for Ψ 5.67° (34) ($\Gamma_{C'(i-1),H\alpha(i-1)C\alpha(i-1)}$), 8.05° (29) ($\Gamma_{H\alpha(i-1)C\alpha(i-1),N(i)HN(i)}$); for φ 6.84° (29) ($\Gamma_{C'(i-1),H\alpha(i)C\alpha(i)}$) and 10.70° (33) ($\Gamma_{H\alpha(i)C\alpha(i),N(i)HN(i)}$), deviations for Σ were slightly higher, i.e., 11.79° (33). The ${}^{3}J_{C'(i)C'(i+1)}$ coupling constant shows an rmsd of 6.40° (35). Direct comparison of deviations in angles in the single experiments with those extracted by the combined use thereof for the two well-defined residues Lys6 and Ala28 reveals that, although somewhat erroneous rates may yield wrong angles if single rates are used, rather exact angles are found upon combination (see Table 5). This finding is also in accordance with the Monte Carlo error analysis performed on those residues which yielded errors in angles of about 3° (see Materials and methods). Generally, the deviation in one rate – if not too extreme – may result in a significant decrease in the Z-value, but will not necessarily shift the extracted maximum position, since one rate presents only a small bias to the fitting procedure. The scatter

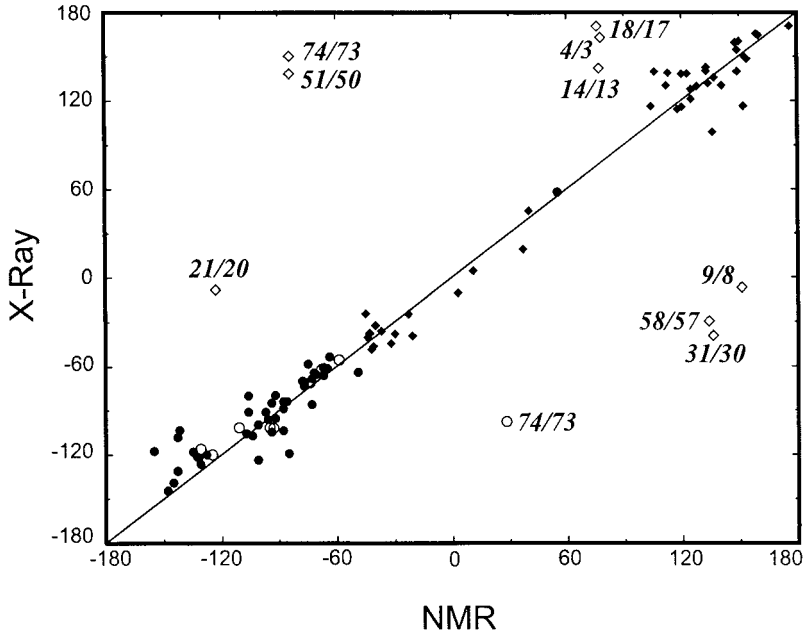

Figure 6. Correlation between values of φ (circles) and ψ (diamonds) determined from Z-surface analysis (NMR) and from the X-ray structure of ubiquitin (X-Ray) (Vijay-Kumar et al., 1987). The Z-surface analysis employed $^3J_{C'C'}$ scalar coupling constants, CSA/dipole ($\Gamma_{C'(i-1),C\alpha(i)H\alpha(i)}$ and $\Gamma_{C'(i),C\alpha(i)H\alpha(i)}$) and dipole/dipole ($\Gamma_{H\alpha(i)C\alpha(i),H(i)N(i)}$, $\Gamma_{H\alpha(i-1)C\alpha(i-1),H(i)N(i)}$ and $\Gamma_{C\alpha(i-1)H\alpha(i-1),C\alpha(i)H\alpha(i)}$) cross-correlation rates. Peptide planes which showed significant deviations are depicted as open symbols and are labeled according to their residue position (see text).

in angles observed over the whole protein can be ascribed to the neglect of contributions from a second cross-correlation rate in the $\Gamma_{C'(i-1),H\alpha(i-1)C\alpha(i-1)}$, $\Gamma_{C'(i-1),H\alpha(i)C\alpha(i)}$, and the $\Gamma_{H\alpha(i)C\alpha(i),H\alpha(i-1)C\alpha(i-1)}$ experiments, variations in the magnitude and orientation of CSA tensor components in case of CSA/DD experiments, and intramolecular motion.

In order to account for the influence of intramolecular dynamics, we corrected the experimental cross-correlation rates by taking into account ^{15}N relaxation data (i.e., experimental cross-correlation rates were divided by the ^{15}N order parameter) prior to the fitting procedure. Of course, this is a simplification, since dynamics of vectors other than N-H^N cannot be assumed to be reflected by ^{15}N order parameters, and as such, this correction may not be sufficient. To assess the influence of internal dynamics on the extracted angles, more sophisticated motional models have been used to generate data sets which were in turn subjected to the Z-surface procedure. The first model assumed harmonic motion around the Cα(i − 1)-C′(i − 1) and the N(i)-Cα(i) bonds, respectively, leading to averaging of the backbone dihedral angles φ and Ψ; this redefines Karplus coefficients according to a parameter σ that reflects the width of a Gaussian distribution around the respective dihedral angle (Brüschweiler and Case, 1994):

$$A^* = A\exp(-2\sigma^2), \tag{11a}$$

$$B^* = B\exp(-\sigma^2/2), \tag{11b}$$

$$C^* = A/2[1-\exp(-2\sigma^2)] + C. \tag{11c}$$

Data were calculated assuming dihedral angle values for two representative residues Lys6 and Ala28, with σ being varied for both angles in a parallel manner in steps of 5° ranging up to 30° for both φ(i) and Ψ(i − 1), whereas averaging around the C^α(i)-C^α(i − 1) axis (affecting Σ(i)) was assigned a parameter σ = 0° (representing the bond vectors Cα(i)-Hα(i) and Cα(i − 1)-Hα(i − 1) as fixed with respect to each other, whereas the encased peptide plane fluctuates). The second model tested was the GAF model (Brüschweiler and Wright, 1994) with motion only around the C^α(i)-C^α(i − 1) axis. Here, cross-correlation order parameters were calculated that depend on the projections of the individual vectors onto the axis of rotation (Brüschweiler and Wright, 1994):

$$S^2 = 1 - 3\sin\theta_1\sin\theta_2\{\cos\theta_1\cos\theta_2[1-\exp(-\sigma^2)] + 1/4\sin\theta_1\sin\theta_2[1-\exp(-4\sigma^2)]\}. \tag{12}$$

Data were created for steps of 5° up to 30°. It could be shown that individual rates may vary significantly over this range. For Lys6 (located in a β-sheet with angles $\varphi(i)/\Psi(i-1) = -95°/114°$), the differences between exact angles and angles extracted for $\sigma = 20°$ are $(-7.2°/+7.5°)$ for the isotropic model and $(-18°/+6.5°)$ for the GAF model, and Z-values drop from 1 to 0.76 and 0.07, respectively. Influence of averaging and motion on rates of Ala28 (located in the α-helix, $\varphi(i)/\Psi(i-1) = -66°/-38°$) are somewhat less pronounced, angles change by $(+2°/-5°)$ and $(-2°/+8°)$, respectively, and Z-values drop from 1 to 0.96 and 0.60 for the two models. The impact of the first model on cross-correlation rates derives from the shape of the theoretical relationships (represented by the Karplus relations). Harmonic motion as encountered in this model results in smoothing of the curves, the extent of which is dependent on the dihedral angles; generally, in 'flat' regions, large alterations should be expected, whereas the influence is less pronounced in the steeper parts. Therefore, the modifications expected for an α-helix are generally small, whereas extended conformations ($\varphi, \Psi \approx -100°/120°$) are expected to vary to a larger extent. GAF like motion (Brüschweiler and Wright, 1994), on the contrary, is determined by projections of vectors onto the Cα(i)-Cα(i − 1)-axis, rendering extended conformations more sensitive to such dynamics than α-helices (where rates determining Ψ are almost unaffected in the GAF model), especially in the CSA/DD experiments. In any case, the effect on extracted angles is minor unless local dynamics are unusually high. According to these preliminary simulations as well as to the experimental findings that deviations may compensate upon combining experiments, we do not expect moderate dynamics to deteriorate the applicability of the procedure. However, residues with substantially smaller than average ^{15}N heteronuclear NOE values and larger than average ^{15}N T_1/T_2 ratios should be discarded from the analysis.

Conclusion

In summary, two new pulse sequences have been proposed for measuring $\Gamma_{H\alpha(i)C\alpha(i),H(i)N(i)}$ and $\Gamma_{H\alpha(i-1)C\alpha(i-1),H(i)N(i)}$ dipole/dipole relaxation interference in ^{15}N,^{13}C-labeled proteins. The experiments have improved sensitivity due to refocusing of passive $^{1,2}J_{NC\alpha}$ scalar couplings. Together with existing methods for the quantification of CSA/dipole relaxation interferences, backbone dihedral angle probability surfaces can be obtained with high degrees of confidence. In many cases, a simultaneous interpretation of $\Gamma_{H\alpha(i)C\alpha(i),H(i)N(i)}$, $\Gamma_{H\alpha(i-1)C\alpha(i-1),H(i)N(i)}$ and $\Gamma_{C\alpha(i-1)H\alpha(i-1),C\alpha(i)H\alpha(i)}$ dipole/dipole, $\Gamma_{C'(i-1),C\alpha(i)H\alpha(i)}$ and $\Gamma_{C'(i),C\alpha(i)H\alpha(i)}$ CSA/dipole cross-correlation rates and $^3J_{C'C'}$ scalar couplings can be used to unambiguously determine backbone dihedral angles in ^{13}C,^{15}N-labeled proteins. Extensions of the method to partially folded and/or unfolded states are straightforward and currently under investigation in our laboratory.

Acknowledgements

The authors thank Prof A.J. Wand (University of Pennsylvania) for kindly supplying uniformly ^{13}C,^{15}N-labeled ubiquitin. R.K. thanks Prof B. Kräutler (University of Innsbruck) for his continuous support. This research was supported by grant P 13486 from the Austrian Science Foundation FWF.

References

Abragam, A. (1986) In *The Principles of Nuclear Magnetism*, Clarendon Press, Oxford.
Bax, A. and Ikura, M. (1991) *J. Biomol. NMR*, **1**, 99–104.
Blommers, M.J.J., Stark, W., Jones, C.E., Head, D., Owen, C.E. and Jahnke, W. (1999) *J. Am. Chem. Soc.*, **121**, 1949–1953.
Boisbouvier, J., Brutscher, B., Pardi, A., Marion, D. and Simorre, J.P. (2000) *J. Am. Chem. Soc.*, **122**, 6779–6780.
Bremi, T. and Brüschweiler, R. (1997) *J. Am. Chem. Soc.*, **119**, 6672–6673.
Brüschweiler, R. and Case, D. A.(1994) *J. Am. Chem. Soc.*, **116**, 11199–11200.
Brüschweiler, R. and Wright, P. E.(1994) *J. Am. Chem. Soc.*, **116**, 8426–8427.
Carlomagno, T., Felli, I.C., Czech, M., Fischer, R., Sprinzl, M. and Griesinger, C. (1999) *J. Am. Chem. Soc.*, **121**, 1945–1948.
Chiarparin, E., Pelupessy, P., Ghose, R. and Bodenhausen, G. (1999) *J. Am. Chem. Soc.*, **121**, 6876–6883.
Chiarparin, E., Pelupessy, P., Ghose, R. and Bodenhausen, G. (2000) *J. Am. Chem. Soc.*, **122**, 1758–1761.
Chiarparin, E., Rüdisser, S. and Bodenhausen, G. (2001) *Chem. Phys. Chem.*, **2**, 41–45.
Cordier, F. and Grzesiek, S. (1999) *J. Am. Chem. Soc.*, **121**, 1601–1602.
Cornilescu, G., Delaglio, F. and Bax, A. (1999), *J. Biomol. NMR*, **13**, 289–302.
Cornilescu, G., Marquardt, J.L., Ottiger, M. and Bax, A. (1998) *J. Am. Chem. Soc.*, **120**, 6836–6837.
Delaglio, F., Grzesiek, S., Vuister, G.W., Zhu, G., Pfeifer, J. and Bax, A. (1995) *J. Biomol. NMR*, **6**, 277–293.
Felli, C., Richter, C., Griesinger, C. and Schwalbe, H. (1999) *J. Am. Chem. Soc.*, **121**, 1956–1957.

Fischer, M.W.F., Zeng, L., Pang, Y., Hu, W., Majumdar, A. and Zuiderweg, E.R.P. (1997) *J. Am. Chem. Soc.*, **119**, 12629–12642.
Garrett, D.S., Powers, P., Gronenborn, A.M. and Clore, G.M. (1991) *J. Magn. Reson.*, **95**, 214–220.
Geen, H. and Freeman, R. (1991) *J. Magn. Reson.*, **93**, 93–141.
Goldman, M. (1984) *J. Magn. Reson.*, **60**, 437–452.
Hu, J.-S. and Bax, A. (1996), *J. Am. Chem. Soc.*, **118**, 8170–8171.
Johnson, B.A. and Blevins, R.A. (1994) *J. Biomol. NMR*, **4**, 603–614.
Junker, J., Reif, B., Steinhagen, H., Junker, B., Felli, I.C., Reggelin, M. and Griesinger, C. (2000) *Chem. Eur. J.*, **6**, 3281–3286.
Kamath, U. and Shriver, J.W. (1989) *J. Biol. Chem.*, **264**, 5586–5592.
Kay, L.E., Ikura, M., Tschudin, R. and Bax, A. (1990) *J. Magn. Reson.*, **89**, 496–514.
Kay, L.E., Keifer, P. and Saarinen, T. (1992) *J. Am. Chem. Soc.*, **114**, 10663–10665.
Kloiber, K. and Konrat, R. (2000a) *J. Biomol. NMR*, **17**, 265–268.
Kloiber, K. and Konrat, R. (2000b) *J. Am. Chem. Soc.*, **122**,12033–12034.
Kloiber, K., Schüler, W. and Konrat, R. (2001) *J. Biomol. NMR.*, **19**, 347–354.
Kupce, E. and Freeman, R. (1995) *J. Magn. Reson.*, **A115**, 273–276.
Kupce, E., Boyd, J. and Campbell, I.D. (1995) *J. Magn. Reson.*, **B106**, 300–303.
Le, H.-B., Pearson, J.G., de Dios, A.C. and Oldfield, E. (1995) *J. Am. Chem. Soc.*, **117**, 3800–3807.
Marion, D., Ikura, M., Tschudin, R. and Bax, A. (1989) *J. Magn. Reson.*, **85**, 393–399.
McCoy, M.A. and Mueller, L. (1992) *J. Magn. Reson.*, **98**, 674–679.
Nilges M., Macias, M.J., O'Donoghue, S.I. and Oschkinat, H. (1997), *J. Mol. Biol.*, **269**, 408–422.
Palmer, A.G.III, Rance, M. and Wright, P.E. (1991) *J. Am. Chem. Soc.*, **113**, 4371–4380.
Pang, Y., Wang, L., Pellecchia, M., Kurochkin, A.V. and Zuiderweg, E.R.P. (1999) *J. Biomol. NMR*, **14**, 297–306.
Pellecchia, M., Pang, Y., Wang, L., Kurochkin, A.V., Kumar, A. and Zuiderweg, E.R.P. (1999) *J. Am. Chem. Soc.*, **121**, 9165–9170.
Pelupessy, P., Chiarparin, E., Ghose, R. and Bodenhausen, G. (1999) *J. Biomol. NMR*, **14**, 277–280.
Reif, B., Diener, A., Hennig, M., Maurer, M. and Griesinger, C. (2000) *J. Magn. Reson.*, **143**, 45–68.
Reif, B., Hennig, M. and Griesinger, C. (1997) *Science*, **276**, 1230–1233.
Reif, B., Steinhagen, H., Junker, B., Reggelin, M. and Griesinger, C. (1998) *Angew. Chem.*, **110**, 2006–2009.
Richter, C., Griesinger, C., Felli, C., Cole, P., Varani, G. and Schwalbe, H. (1999) *J. Biomol. NMR*, **15**, 241–250.
Schleucher, J., Sattler, M. and Griesinger, C. (1993) *Angew. Chem. Int. Ed. Engl.*, **32**, 1489–1491.
Shaka, A.J., Keeler, J., Frenkiel, T. and Freeman, R. (1983) *J. Magn. Reson.*, **52**, 335–338.
Skrynnikov, N.R., Konrat, R., Muhandiram, D.R. and Kay, L.E. (2000) *J. Am. Chem. Soc.*, **122**, 7059–7071.
Sprangers, R., Bottomley, M.J., Linge, J.P., Schultz, J., Nilges, M. and Sattler, M. (2000) *J. Biomol. NMR*, **16**, 47–58.
Teng, Q., Iqbal, M. and Cross, T.A. (1992) *J. Am. Chem. Soc.*, **114**, 5312–5321.
Tjandra, N. and Bax, A. (1997) *J. Am. Chem. Soc.*, **119**, 9576–9577.
Tjandra, N., Feller, S.E., Pastor, R.W. and Bax, A. (1995) *J. Am. Chem. Soc.*, **117**, 12562–12566.
Tolman, J.R., Chiarparin, E. and Bodenhausen, G. (2000) *J. Am. Chem. Soc.*, **122**, 11523–11524.
Vijay-Kumar, S., Bugg, C.E. and Cook, W.J. (1987) *J. Mol. Biol.*, **194**, 531–544.
Vuister, G.W. and Bax, A. (1992) *J. Magn. Reson.*, **98**, 428–435.
Vuister, G.W., Delaglio, F. and Bax, A. (1992) *J. Am. Chem. Soc.*, **114**, 9674–9675.
Wand, A.J., Urbauer, J.L., McEvoy, R.P. and Bieber, R.J. (1996) *Biochemistry*, **35**, 6116–6125.
Yang, D. and Kay, L.E. (1998) *J. Am. Chem. Soc.*, **120**, 9880–9887.
Yang, D., Gardner, K.H. and Kay, L.E. (1998) *J. Biomol. NMR*, **11**, 1–8.
Yang, D., Konrat, R. and Kay, L.E. (1997) *J. Am. Chem. Soc.*, **119**, 11938–11940.
Ye, C., Fu, R., Hu, J., Hou, L. and Ding, S. (1993) *Magn. Reson. Chem.*, **31**, 699–704.